**Article:**
Wallis, R., Simmonite, E., Cooper, H. et al. (2026) Variable mitochondrial phenotypes and reduced complex IV assembly factor SCO2 in LRRK2-G2019S fibroblasts. Scientific Reports. ISSN: 2045-2322

https://doi.org/10.1038/s41598-026-58797-0

Scientific Reports

https://doi.org/10.1038/s41598-026-58797-0

Article in Press

# Variable mitochondrial phenotypes and reduced complex IV assembly factor SCO2 in *LRRK2*-G2019S fibroblasts

Received: 5 March 2026

Accepted: 16 June 2026

Published online: 25 June 2026

Cite this article as: Wallis R., Simmonite E., Cooper H. *et al.* Variable mitochondrial phenotypes and reduced complex IV assembly factor SCO2 in *LRRK2*-G2019S fibroblasts. *Sci Rep* (2026). https://doi.org/10.1038/s41598-026-58797-0

**Ruby Wallis, Ella Simmonite, Harry Cooper, Olivia Cracknell, Amandeep Kaur, Elizabeth J. New, Jan Aasly, Oliver Bandmann & Heather Mortiboys**

# Variable mitochondrial phenotypes and reduced complex IV assembly factor SCO2 in *LRRK2*-G2019S fibroblasts

Ruby Wallis[1], Ella Simmonite[1], Harry Cooper[1], Olivia Cracknell[1], Amandeep Kaur[2,3], Elizabeth J. New[3], Jan Aasly[4†], Oliver Bandmann[1,5], Heather Mortiboys[1,5]

**Affiliations**

1. Sheffield Institute for Translational Neuroscience (SITraN), School of Medicine and Population Health, Faculty of Health, University of Sheffield, 385a Glossop Road, Sheffield, S10 2HQ
2. School of Chemistry, The University of Sydney, NSW 2006, Australia
3. Current affiliation: Medicinal Chemistry, Monash Institute of Pharmaceutical Sciences Monash University, Parkville, VIC 3052, Australia
4. Department of Neurology, St Olav's Hospital, Trondheim, Norway
5. Neuroscience Institute, University of Sheffield, Western Bank, Sheffield

† deceased

ruby.wallis@ukdri.ac.uk
ersimmonite1@sheffield.ac.uk
hcooper1102@gmail.com
olivia.cracknell@babraham.ac.uk
a.kaur@monash.edu
elizabeth.new@sydney.edu.au
o.bandmann@sheffield.ac.uk
h.mortiboys@sheffield.ac.uk

**Corresponding Author:**

Professor Heather Mortiboys
Sheffield Institute for Translational Research (SITraN)
School of Medicine and Population Health
University of Sheffield
385a Glossop Road
Sheffield
S10 2HQ
H.Mortiboys@sheffield.ac.uk



## Abstract

**Background**: *LRRK2*-G2019S is the most common pathogenic *LRRK2* mutation which accounts for up to 13% of cases of familial Parkinson's disease. The *LRRK2*-G2019S mutation has incomplete penetrance which increases with age. Molecular mechanisms which contribute to the disease status in *LRRK2*-G2019S mutation carriers are yet to be fully defined. Here, we aimed to further investigate the specific mitochondrial effects of *LRRK2*-G2019S penetrance in a cohort of patient-derived fibroblasts from manifesting and non-manifesting *LRRK2*-G2019S carriers compared to controls to further elucidate the pathogenic mechanism of the mutation.

**Results**: We find a significant reduction of 50% in the expression of the complex IV assembly factor SCO2 in *LRRK2*-G2019S manifesting fibroblasts. In contrast, SCO2 levels remained similar to controls in non-manifesting *LRRK2*-G2019S carriers. A small reduction in complex IV subunit expression accompanied this reduction in SCO2 in manifesting *LRRK2*-G2019S. Despite the role of SCO2 in copper incorporation into complex IV, we identified no differences in the unbound mitochondrial copper content in a limited number of manifesting or non-manifesting *LRRK2*-G2019S carriers compared to controls. However,

*LRRK2*-G2019S carriers exhibit variable cellular phenotypes in mitochondrial morphology, mitochondrial membrane potential and cellular ATP or ROS production which does not differ significantly between manifesting and non-manifesting carriers.

**Conclusions**: We conclude that mitochondrial complex IV deficiency could be a pathogenic mechanism of the *LRRK2*-G2019S mutation which may be attributed to a reduction in SCO2, however there is evident heterogeneity in the cellular phenotype of *LRRK2*-G2019S carriers which may suggest underlying compensatory mechanisms.

**Keywords:** Leucine-Rich Repeat Kinase-2 (LRRK2), G2019S mutation, mitochondria, Parkinson's disease, penetrance, manifesting, non-manifesting

## Background

The global prevalence of Parkinson's disease (PD) has doubled in the past 25 years (1)(2). Depositions of aggregated α-synuclein (α-syn) within Lewy bodies (LBs) in the substantia nigra pars compacta (SNc) are the main pathological hallmarks and contribute to the progressive loss of dopaminergic neurons. Neuronal loss ultimately leads to the symptoms which include the classical motor symptoms of tremors and bradykinesia, as well as non-motor symptoms (3). Increasing age is the most prevalent risk factor for the development of PD (4). In familial PD, age of onset can also differ between the genetic forms; parkin-related PD is associated with early onset, with a median age of onset of 31 years (5).

Mutations in the Leucine-Rich Repeat Kinase 2 (*LRRK2*) accounts for 5-13% of familial PD and 1-5% of sporadic PD (6)(7). LRRK2 PD however has a comparable age of onset to idiopathic PD; typically, over 50 years of age (8). The most common pathogenic *LRRK2* mutation is the *LRRK2*-Gly2019Ser (G2019S) variant, which resides in the kinase domain of LRRK2 and results in increased kinase activity (9)(10).

*LRRK2*-G2019S is present in 1% of sporadic PD cases and over 4% of familial cases worldwide (11). However, previous evidence highlights that the LRRK2-G2019S mutation does not have complete penetrance, suggesting that other risk factors may influence the onset of PD within *LRRK2*-G2019S mutation carriers. The reported penetrance of the mutation is inconsistent across different studies and particularly across different populations throughout the world, however, most report the same trend of an increase in penetrance with age. *LRRK2*-G2019S penetration has been reported at ~28% at 59 years of age, increasing to ~67-74% at ages over 79 (11)(12). The incomplete penetrance of the mutation highlights the importance of studying cohorts who have the *LRRK2*-G2019S mutation and do not currently have PD symptoms (non-manifesting) alongside those who have the mutation and are clinically diagnosed with PD (manifesting), to broaden our understanding of the changes occurring with the mutation and identify which could be pathogenic.

The 286 kDa protein, LRRK2, has roles in the regulation of autophagy, cytoskeletal dynamics and many other cellular pathways. It can also directly affect mitochondrial function as approximately 10% of LRRK2 localises with the outer mitochondrial membrane (10)(13)(14)(15). Previous work has identified multiple mitochondrial abnormalities in *LRRK2*-G2019S manifesting and non-manifesting fibroblasts when compared to controls; these include reduced mitochondrial membrane potential (MMP), decreased ATP production and mitochondrial morphological changes including increased mitochondrial elongation (16)(17). In addition, specific reductions in mitochondrial respiratory chain complex III and IV activity in fibroblasts from *LRRK2*-G2019S non-manifesting and manifesting PD patients has been reported (16)(17). The cerebral cortex of *LRRK2*-G2019S PD mice also show altered mitochondrial morphology, and the striatum of *LRRK2*-G2019S knock-in mice exhibit a 10% increase in mitochondrial length and a significant reduction in mitochondrial number

compared to WT (18)(19). The protein DRP1, responsible for LRRK2-mediated mitochondrial fission, is elevated in brain lysates of *LRRK2*-G2019S transgenic mice, suggesting a possible mechanism of LRRK2 mediated mitochondrial alteration via DRP1 in PD (20).

Although there are currently no disease modifying treatments for PD, in recent years there has been substantial progress in the development of therapeutics for LRRK2-PD, including advances in the development of antisense oligonucleotides (ASOs). LRRK2-specific ASOs act via binding target mRNA and subsequent mRNA degradation, thus suppressing LRRK2 activity (21)(22). ION859, formerly known as BIIB094, is the first ASO to reach clinical phase development for the treatment of LRRK2-PD and has recently successfully completed a phase 1 safety and tolerability trial in LRRK2-PD patients (NCT03976349, clinicaltrials.gov). An alternative approach aims to reduce kinase activity via the development of specific kinase inhibitors. The most advanced of these is BIIB122, currently in a phase 2 clinical trial for early-stage PD (NCT05348785, clinicaltrials.gov). Multiple other LRRK2 kinase inhibitors have been developed and used for pre-clinical research LRRK2 cellular models and some of these have proved effective in cellular models of altering mitochondrial morphological changes (20). Another specific kinase inhibitor selective for G2019S mutant LRRK2, EB-42168, has shown reversal of mitochondrial DNA damage. However, mitophagy, which can be defective in *LRRK2*-G2019S PD, was not altered by the inhibitor (23). Overall, the mechanisms leading to the mitochondrial abnormalities caused by LRRK2 remain largely unknown; furthermore, the mitochondrial phenotype may vary depending on model, cell type, and patient, therefore more work is required to understand the mitochondrial impairment and involvement in LRRK2-PD.

This study aims to address some of these unanswered questions relating to mitochondrial dysfunction in LRRK2-PD. Here we focus on patient derived cell models, expanding into a larger cohort of *LRRK2*-G2019S manifesting, non-manifesting and control fibroblasts. We assessed functional parameters including MMP, ATP levels and the overall protein expression of mitochondrial respiratory chain complexes and fission/fusion factors. We also investigated the effect of *LRRK2*-G2019S on other mitochondrially related pathways including copper insertion and reactive oxygen species (ROS) production. Herein we propose a mechanism by which the complex IV deficiency is caused by the *LRRK2* mutation.

## Results

### ATP levels in *LRRK2*-G2019S manifesting and non-manifesting fibroblasts show a mixed profile

Production of ATP by the mitochondria is essential in fulfilling the cell's metabolic requirements. Fibroblasts have relatively low metabolic requirements in comparison to other cell types such as dopaminergic neurons, and mainly rely on glycolysis to generate ATP, particularly under glucose-rich cell culture conditions. As well as glycolysis, ATP can also be generated at higher net levels through oxidative phosphorylation in the mitochondria. To direct fibroblasts to generate more of their ATP using oxidative phosphorylation, and thereby measure mitochondrial function, fibroblasts can be grown in galactose-containing media (17). Indeed, fibroblasts with severe respiratory defects have reduced survival when cultured in galactose containing media (33).

Our previous study of a set of *LRRK2*-G2019S fibroblasts showed significantly reduced ATP levels compared to control cells (16). Here we measured total cellular ATP levels in an additional cohort of cell lines. None of the G2019S lines (neither non-manifesting nor manifesting) showed alterations in ATP when grown in glucose media (Figure 1a). However, non-manifesting-4 had a significant reduction in ATP levels when cultured in galactose

media (66% mean reduction compared with controls in galactose media; Figure 1a, p=0.0109). Manifesting-1 also showed a trend towards a decrease in ATP levels (36% mean reduction compared with controls in galactose media), though did not reach significance in this small cohort (p=0.24). Figure 1b shows the percentage change in ATP levels when cells are cultured in galactose media compared with glucose media. The controls show an increase in ATP when switched to galactose media, as would be expected, as oxidative phosphorylation has a higher net production of ATP than glycolysis. The non-manifesting-3 and manifesting-1 cell lines show no difference between media types, and ATP levels are significantly decreased in non-manifesting-4 when cultured in galactose media (p=0.0036), suggesting a defect in oxidative phosphorylation.

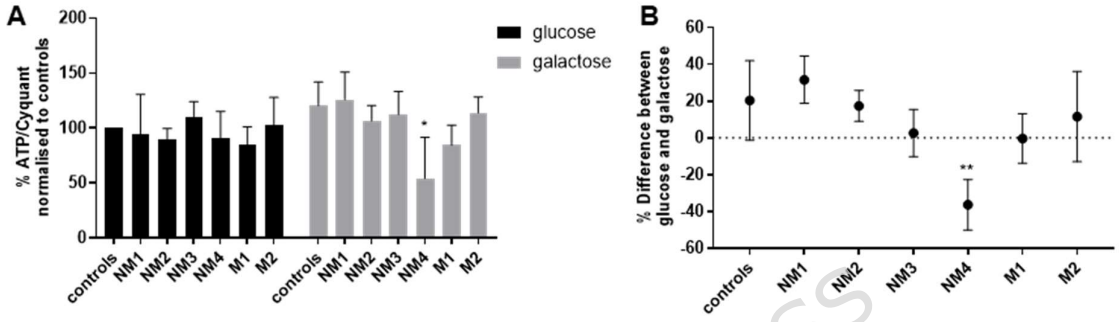


**Figure 1 - ATP levels in *LRRK2*-G2019S manifesting, non-manifesting and control fibroblasts.** *LRRK2*-G2019S manifesting (M), *LRRK2*- G2019S non-manifesting (NM), control (C) n=3 control lines pooled. (**a**) Percentage of total cellular ATP/Cyquant normalised to glucose media controls. (**b**) Percentage difference in normalised total cellular ATP levels between glucose and galactose media. *p<0.05 **p<0.01 one-way ANOVA with Dunnett's multiple comparisons. Each line was repeated at least 3 times, with the exception of 1 control line due to poor growth. Results are expressed as the mean ± SD.

**Mitochondrial membrane potential in *LRRK2*-G2019S manifesting and non-manifesting fibroblasts is unaltered**

As well as measuring total cellular ATP levels, mitochondrial function was also assessed by measuring mitochondrial membrane potential (MMP). Carbonyl cyanide m-chlorophenylhydrazone (CCCP), a mitochondrial uncoupler which disrupts the membrane potential, was used as a positive control of reduced TMRM staining, where the fluorescence intensity of TMRM is visibly decreased with CCCP treatment, compared to the untreated condition (Figure 2a). Mitochondrial area showed variation between cell lines, therefore, we defined the mitochondria by two groups; short mitochondria and long mitochondria. Short mitochondria were defined as having a form factor >0.4 and long mitochondria were defined as having a form factor <0.4. The biological relevance of morphologically different mitochondria is important to consider when assessing turnover of damaged mitochondria, as has been identified in multiple PD models and patient cells. As shown in Figure 2b and 2c, there is no difference in TMRM intensity between most of the cell lines. However, two lines, non-manifesting 2 (short p=0.0204, long p=0.0045) and manifesting-1 (short p=0.0008, long p=0.0003) show an increase in TMRM intensity compared with controls in galactose media. TMRM intensity shows the same pattern between media type and between short and long mitochondria, suggesting that neither media type nor the size of mitochondria is affecting the overall membrane potential.

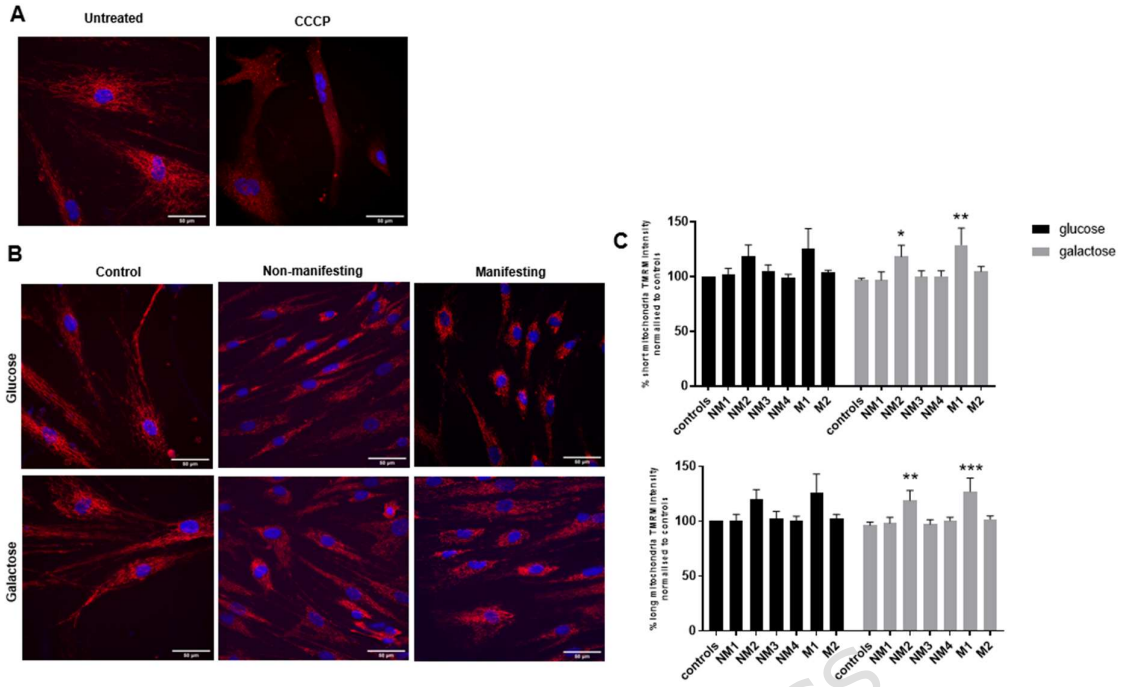


**Figure 2 - Mitochondrial membrane potential in *LRRK2*-G2019S manifesting, non-manifesting and control fibroblasts.** *LRRK2*-G2019S manifesting (M), *LRRK2*-G2019S non-manifesting (NM), control (C) n=3 control lines pooled. Each line was repeated at least 3 times, with 3 technical repeats, with the exception of 1 control line due to poor growth. On average, 150-300 cells per cell line, per condition for each repeat were analysed. (**a**) Representative images of TMRM staining for untreated and CCCP treated fibroblasts. (**b**) Representative images of TMRM staining for control, non-manifesting and manifesting fibroblasts in glucose and galactose media. Scale bar, 50 µm. (**c**) % TMRM intensity normalised to glucose media controls in short (upper) and long (lower) mitochondria. Short mitochondria were defined as having a form factor >0.4 and long mitochondria were defined as having a form factor <0.4 *p<0.05, **p<0.01, ***p<0.001 one-way ANOVA with Dunnett's multiple comparisons. Results are expressed as the mean ± SD

## Mitochondrial and cytosolic reactive oxygen species are unaltered in *LRRK2*-G2019S manifesting and non-manifesting fibroblasts

Previous data has suggested an increase in reactive oxygen species (ROS) in *LRRK2*-G2019S PD cells, as well as altered ATP production in these cells (34). However, there is very little literature exploring ROS in both *LRRK2*-G2019S manifesting and non-manifesting fibroblasts. In this study, we use two mitochondrial ROS probes, FRR2 and NpFR2, and one cytosolic ROS probe, NpFR1 (27)(28)(29). These probes are not selective for specific ROS, but instead provide details of the overall redox status of their environments and their reversibility means they can equilibrate to report on the redox environment. Here, we investigated mitochondrial and cytosolic ROS levels in several *LRRK2*-G2019S manifesting, non-manifesting and control fibroblast cell lines, in both glucose media and after 24 hours in galactose containing media (Figure 3).

Both mitochondrial ROS probes showed a similar pattern of results (Figure 3a and 3b), thus further validating the results presented (Figure 3c and 3d). There was no significant change in mitochondrial ROS between the different subgroups (glucose media manifesting, 101 ± 19%; glucose media non-manifesting, 89 ± 14%; galactose media manifesting, 109 ± 21%; galactose media non-manifesting, 91 ± 12%, galactose media control 100 ± 11%; Figure 3c). Interestingly, the LRRK2-manifesting line which did not have an ATP defect, had the lowest mitochondrial ROS levels of the manifesting lines (Figure 3c). Some of the other *LRRK2*-G2019S manifesting lines showed a small increase in mitochondrial ROS compared to controls, while the non-manifesting lines had a trend towards a decrease, as can be seen from the triplicate experimental repeats in Figure 3c. However, this data was variable

between patient lines (Supplementary Figure 1). No differences were observed between the different subgroups when assessing cytosolic ROS (Figure 3e and 3f).

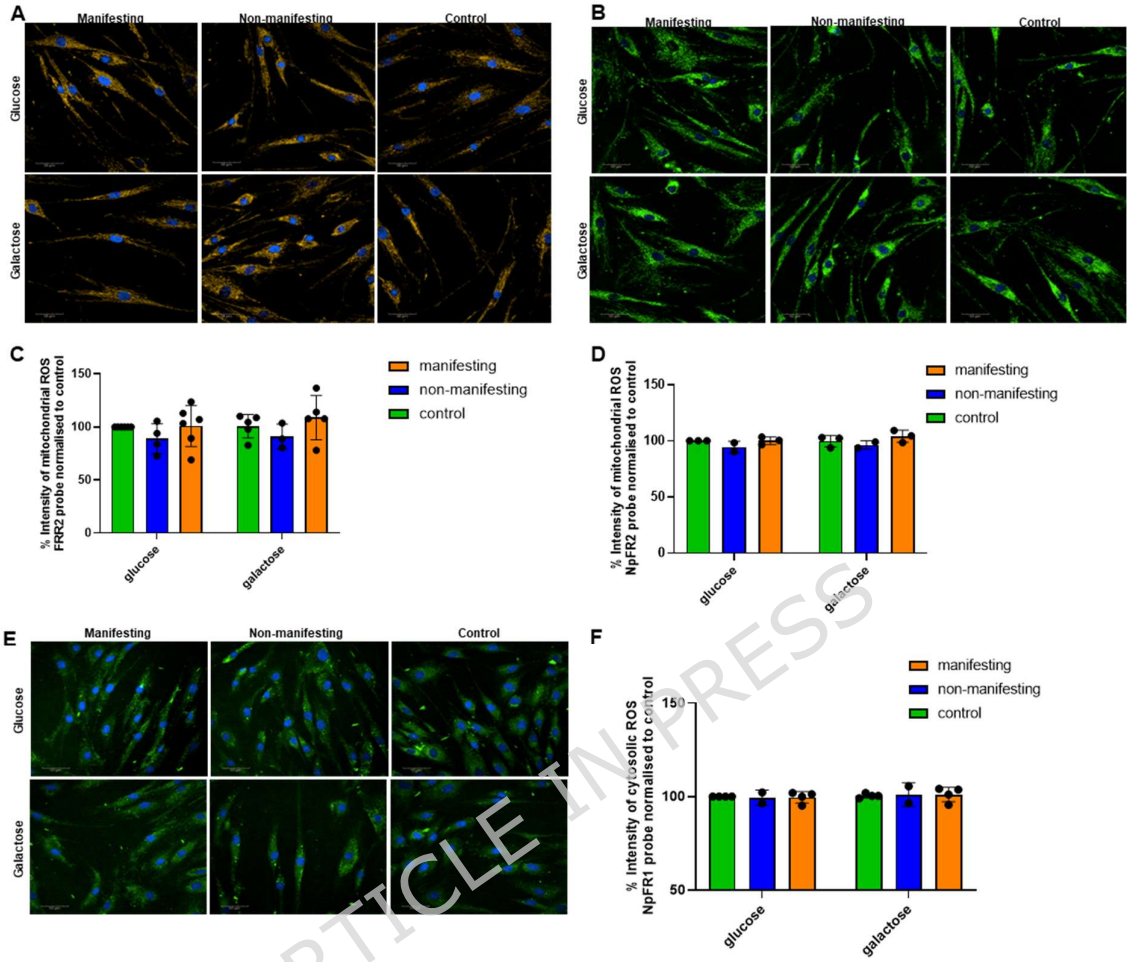


**Figure 3 - Mitochondrial and cytosolic reactive oxygen species levels in *LRRK2*-G2019S manifesting, non-manifesting and control fibroblasts.** (**a**) Representative images of mitochondrial ROS probe FRR2 (orange) and (**b**) NpFR2 (green) in LRRK2-G2019S manifesting, non-manifesting and control fibroblasts in glucose and galactose media. (**c**) Quantification of FRR2 intensity normalised to glucose media controls. n = 6 *LRRK2*-G2019S manifesting, 4 *LRRK2*-G2019S non-manifesting, 7 control fibroblast lines in glucose media and 5 *LRRK2*-G2019S manifesting, 3 *LRRK2*-G2019S non-manifesting, 5 control fibroblast lines in galactose media. (**d**) Quantification of NpFR2 intensity normalised to glucose media controls. n = 3 *LRRK2*-G2019S manifesting, 2 *LRRK2*-G2019S non-manifesting, 4 control fibroblast lines in both media types. (**e**) Representative images of cytosolic ROS probe NpFR1 (green) in *LRRK2*-G2019S manifesting, non-manifesting and control fibroblasts in glucose and galactose media. (**f**) Quantification of NpFR1 intensity normalised to glucose media controls,. n = 4 *LRRK2*-G2019S manifesting, 2 *LRRK2*-G2019S non-manifesting, 5 control fibroblast lines in both media types. Each dot represents the mean of the experimental repeats per line for lines with at least 2 biological repeats, apart from 1 control and 1 manifesting for NpFR1 in the galactose condition. On average, 150-300 cells per cell line, per condition for each repeat were analysed. Results are expressed as the mean ± SD. Scale bar, 50 µm.

## Mitochondrial morphology is altered in *LRRK2*-G2019S manifesting and non-manifesting fibroblasts

In addition to functional mitochondrial differences, like MMP, changes in mitochondrial morphology have also been implicated in *LRRK2*-G2019S cells (16)(35)(36). Therefore, we also analysed mitochondrial morphology. Figure 4a shows a significant increase in mitochondrial count per cell area for both non-manifesting and manifesting groups compared to controls in both media types. There was also an increase in the percentage of perinuclear mitochondria, an indicator of cellular stress, by a mean of 115% and 119% (p=0.0112), in non-manifesting and 114% and 115% in manifesting compared to controls in glucose and

galactose media, respectively (Figure 4b). Perinuclear mitochondria are defined as within a collar surrounding the nucleus of 15%.

Mitochondria of different sizes are known to have different functions; hence we segmented two mitochondrial populations, short mitochondria and long mitochondria. There was a slightly higher percentage of short mitochondria present in the non-manifesting groups in glucose (102%) and in galactose (109%) compared to controls, alongside an increase in percentage of short mitochondria in manifesting groups in glucose (108%) and galactose (105%) although not significant (Figure 4c). A smaller increase in total mitochondrial area occupied by short mitochondria compared to controls was seen in the non-manifesting group in glucose and galactose media (111%) (Figure 4d). Together, this suggests that certain LRRK2-G2019S manifesting and non-manifesting lines have more fragmented mitochondria compared to controls, which is not influenced by cell size (Supplementary Figure 2).

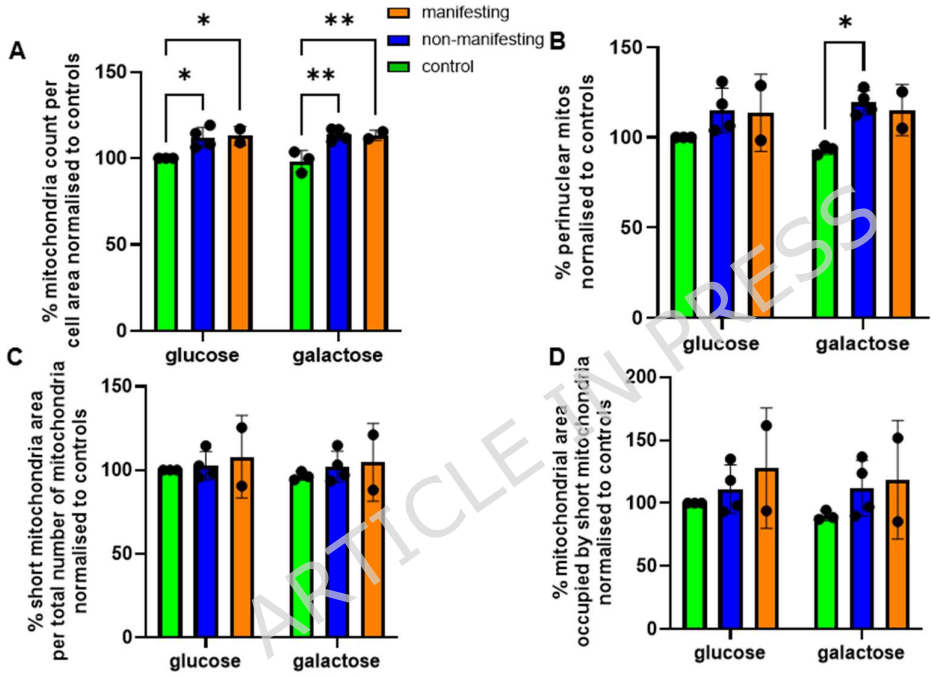


**Figure 4 - Mitochondrial morphology parameters from TMRM staining in *LRRK2*-G2019S manifesting, non-manifesting and control fibroblasts.** *LRRK2*-G2019S manifesting (M) n=2 lines pooled, *LRRK2*-G2019S non-manifesting (NM) n=4 lines pooled, control (C) n=3 control lines pooled. Each dot is mean of the individual cell line from n=3 biological repeats. Each line was repeated at least 3 times at different passages, with 3 technical repeats per biological repeat, with the exception of 1 control line due to poor growth. On average, 150-300 cells per cell line, per condition for each repeat were analysed. (**a**) Mean mitochondria count normalised to glucose media controls. (**b**) Percentage of perinuclear mitochondria normalised to glucose media controls. The perinuclear region is defined as the region which is half of the radius of each nuclei away from the nuclei perimeter. (**c**) Percentage short mitochondria per total number of mitochondria normalised to glucose media controls. (d) Percentage of mitochondria area occupied by short mitochondria normalised to glucose media controls. Results expressed as the mean ± SD. *p<0.05, 2-way ANOVA with Dunnett's multiple comparisons.

## Protein expression of mitochondrial fission and fusion mediators OPA1 and DRP1 is unaltered in *LRRK2*-G2019S manifesting and non-manifesting fibroblasts

After investigating the mitochondrial morphology using fluorescence microscopy we also investigated if these morphological changes were due to alterations in the protein expression of the mitochondrial fission/fusion factors; as changes in these have been implicated in LRRK2 mutant models by others (35)(37)(38).

We investigated expression levels of two proteins; OPA1 and DRP1, which are involved in mitochondria fusion and fission, respectively. Two isoforms of each protein were seen in both OPA1 and DRP1 blots. For OPA1 we quantified relative expression for both isoforms

separately as they produced very distinct bands and there is evidence that the long and short isoforms of OPA1 play different roles in mitochondrial fusion. The long isoform of OPA1 has been shown to be tethered to the inner mitochondrial membrane, which may be more important in the mitochondrial fusion process. Conversely, the short isoform may play a role in mitochondrial fission (39)(40). For DRP1, we quantified both isoforms together as the bands were less distinct and currently the roles of the different isoforms are less well defined than those of OPA1. However, there is evidence that when mitochondrial fission is upregulated, there is a trend towards an increase in the number of large DRP1 oligomers (41). DRP1 is phosphorylated to activate and inactivate however we did not assess this here and the two isoforms are not post translationally modified protein.

No difference was observed in protein expression for either OPA1 isoforms (long isoform manifesting, 109 ± 34%; long isoform non-manifesting, 117 ± 33%; short isoform manifesting, 96 ± 46% ; short isoform non-manifesting, 106 ± 26%) (Figure 5a and 5b), or DRP1 (manifesting 88 ± 28%; non-manifesting, 61 ± 40%), between manifesting, non-manifesting and control fibroblasts. There was, however a decrease in DRP1 expression in the majority of the non-manifesting cell lines. Although, the expression of DRP1 is variable within the different groups, more so than that of other proteins probed in this study (Figure 5c and 5d)(Supplementary Figure 3).

As DRP1 is a cytosolic protein and is recruited to the mitochondrial outer membrane for mitochondrial fission, we also investigated the localisation of DRP1. Figure 5e and 5f show representative staining of the different cell lines, where DRP1 can be seen in both the cytoplasm and localised with TOM20. There were small and variable changes in DRP1 localisation (Figure 5e-h). Overall, these findings suggest minimal changes in DRP1 localization at basal conditions in fibroblasts.

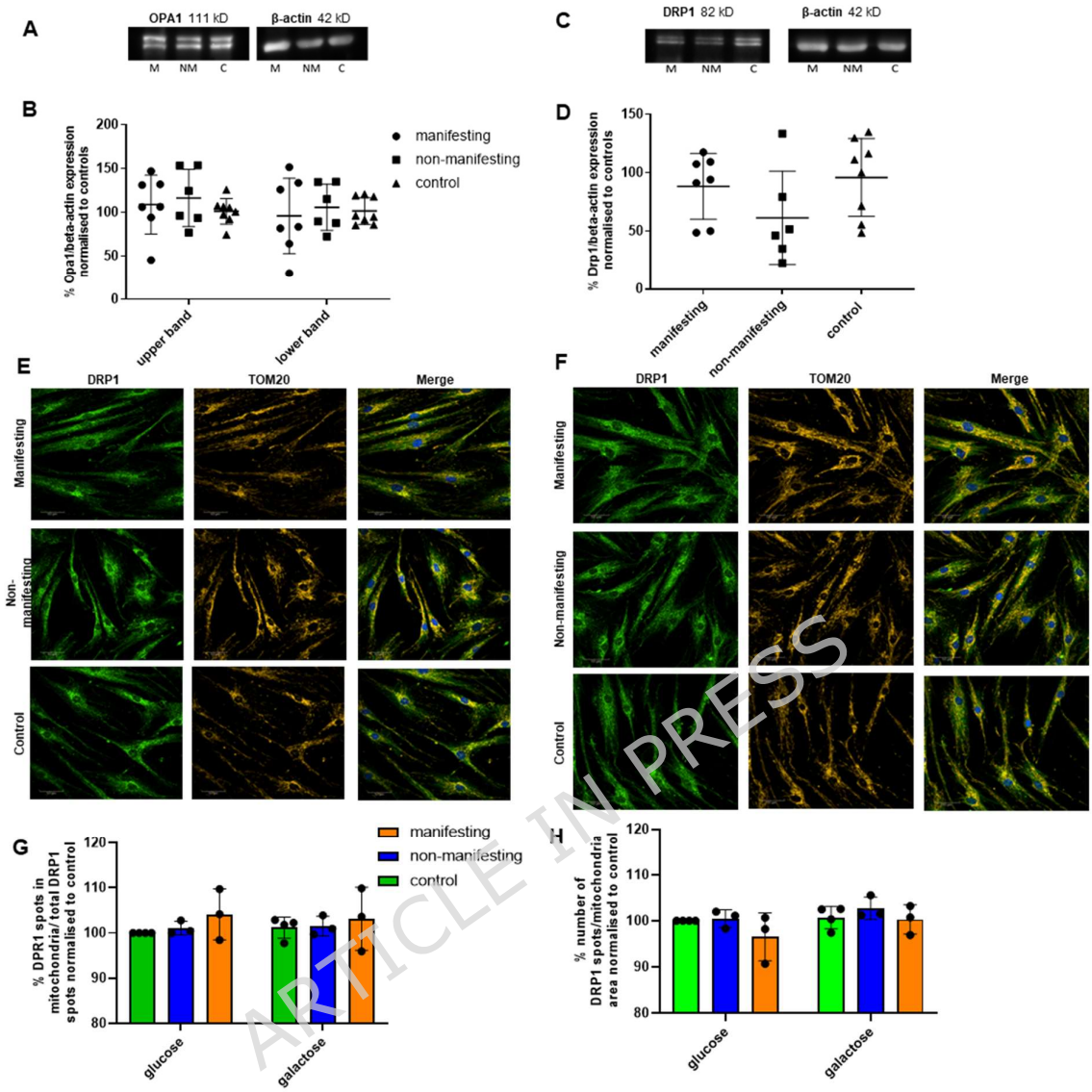


**Figure 5 - Protein expression of OPA1 and DRP1 in *LRRK2*-G2019S and cellular DRP1 localisation staining of DRP1 in manifesting, non-manifesting and control fibroblasts.** (**a**) Representative western blot of OPA1 (111 kDa) and beta actin (42 kDa). (**b**) Quantification of western blots showing the percentage of OPA1/beta-actin expression normalised to controls for upper and lower bands. (**c**) Representative western blot of DRP1 (82 kDa) and beta-actin (42 kDa). (**d**) Quantification of western blots showing the percentage of DRP1l/beta-actin expression normalised to controls. For western blots, n = 7 *LRRK2*-G2019S manifesting (M), 6 *LRRK2*-G2019S non-manifesting (NM), 8 control (C) fibroblast lines from at least 2 experimental repeats per line (**e**) Representative staining images of DRP1 (green) and TOM20 (orange) in *LRRK2*-2019S manifesting, non-manifesting and control fibroblasts. TOM20 was used as a mitochondrial marker and Hoechst (blue) was used to label nuclei. Scale bar, 50 µm. (**e**) cells in glucose media (**f**) cells in galactose-containing media for 24 hours. (**g**) % DRP1 spots in mitochondria per total DRP1 spots normalised to controls in glucose and galactose media. . (**h**) % Number of DRP1 spots per mitochondrial area normalised to glucose media controls. Results are expressed as the mean ± SD, Each dot represents the mean of the experimental repeats per line. For imaging assays, n = 3 *LRRK2*-G2019S manifesting, 3 *LRRK2*-G2019S non-manifesting and, 4 control fibroblast cell lines. Due to cell growth, variable number of experimental repeats were obtained for different control lines, 3 experimental repeats were obtained from 2 controls, 2 experimental repeats of 1 control, and 1 experimental repeat of 1 control. For *LRRK2*- G2019S manifesting and non-manifesting lines 3 experimental repeats were obtained. On average, 150-300 cells per cell line, per condition for each repeat were analysed.

## Reduced protein expression of complex IV assembly factor in *LRRK2*-G2019S manifesting fibroblasts

As we have previously shown a reduction in complex III and IV activity in a subset of this cohort (17), we wanted to explore whether protein expression of the different mitochondrial

oxidative phosphorylation (OXPHOS) complexes was altered, potentially contributing to a decrease in activity. Western blots were performed using an antibody cocktail to look at specific subunits from the five mitochondrial complexes (Figure 6a). The entire cohort of lines was investigated as we have not previously assessed protein levels in any of the cohort, in total 8 controls, 6 non-manifesting and 7 manifesting lines were measured.

The complex I subunit measured using this OXPHOS cocktail antibody, NDUFB8 is particularly labile and could not be visualised on all blots, therefore has a lower sample size than the other complexes. No significant difference was found between either *LRRK2*-G2019S manifesting or non-manifesting fibroblasts compared with controls in any of the OXPHOS subunits. There was a small, but non-significant decrease of 22% in expression of complex IV in the *LRRK2*-G2019S manifesting fibroblasts compared with controls (Figure 6c).

As our data did not show significant reductions in these complexes, we proposed the reduced activity of complex III and IV which we have previously published, may be due to deficits in the assembly of these complexes. There are several known factors involved in the assembly of complexes III and IV. However, this study focused on BCS1L (complex III assembly factor) and SCO2 (complex IV assembly factor) due to both assembly factors being fundamental in the assembly of the core subunits of their respective complexes (42)(43).

As can be seen in Figure 6d and 6e, there was no change in BCS1L protein expression across either the manifesting (108 ± 35%) or non-manifesting groups (80 ± 12%). On the other hand, SCO2 expression levels were significantly reduced (p=0.0139) in the manifesting patient group by a mean of 50% (Figure 6f and 6g). The non-manifesting lines were variable in SCO2 expression, with two lines showing much higher expression levels (Figure 6g). As, manifesting-1 displayed an ATP deficit (Figure 1) along with all *LRRK2*-G2019S manifesting lines published previously by our group (16)(17), and manifesting-2 showed no ATP defect in this study (Figure 1), we decided to exclude this from the analysis in Figure 6c and 6g to thoroughly assess whether lines with an identified ATP deficit show a decrease in SCO2 expression levels,

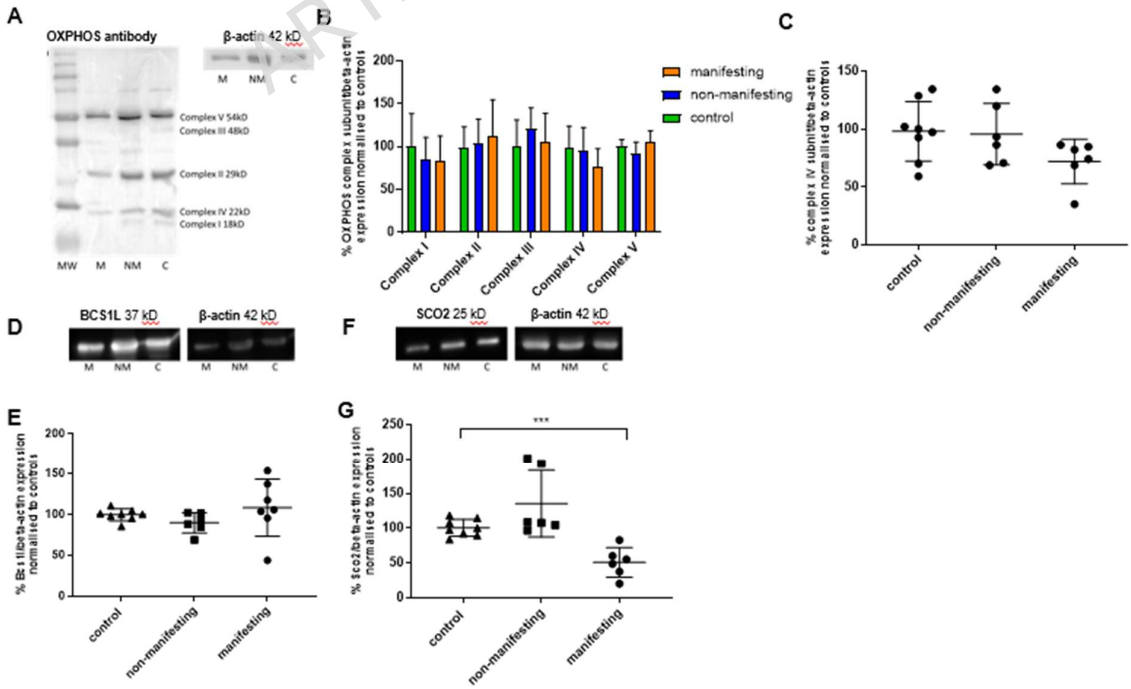

**Figure 6 - Protein expression of OXPHOS complex subunits, BCSL1 and SCO2 in *LRRK2*-G2019S manifesting, non-manifesting and control fibroblasts.**
(**a**) Representative western blot of the mitochondrial complex antibody cocktail and beta-actin (42 kDa). MW, molecular weight marker. (**b**) Quantification of western blots showing the percentage of OXPHOS complex subunit/beta-actin expression normalised to controls. Complex I n= 6 *LRRK2*-G2019S manifesting, 5 *LRRK2*-G2019S non-manifesting, 6 control fibroblasts from at least 2 experimental repeats per line. (**c**) Quantification of complex IV western blot excluding manifesting-2 which has no ATP deficit. (**d**) Representative western blot of BCS1L (48 kDa) and beta-actin (42 kDa). (**e**) Quantification of western blots showing the percentage of Bcs1l/beta-actin expression normalised to controls. (**f**) Representative western blot of SCO2 (25 kDa) and beta-actin (42 kDa). (**g**) Quantification of SCO2 expression excluding manifesting-2 which has no ATP deficit. *p<0.05 Kruskal-Wallis test. For all western blots n=7 *LRRK2*-G2019S manifesting (M), 6 *LRRK2*-G2019S non-manifesting (NM), 8 control (C) fibroblast lines from at least 2 experimental repeats per line, apart from complex I as mentioned above. Results are expressed as the mean ± SD. Each dot represents the mean of the experimental repeats per line.

## Mitochondrial and cytosolic copper in LRRK2 manifesting, non-manifesting and control fibroblasts

Due to the significant reduction of SCO2 expression in *LRRK2*-G2019S manifesting fibroblasts and the fundamental role of SCO2 in incorporating CuA into mitochondrial complex IV, we hypothesised that there may be a change in mitochondrial copper in *LRRK2*-G2019S fibroblasts. To investigate this, a mitochondrial copper probe, InCCu1, was used to assess unbound mitochondrial copper in different cell lines (30). When copper is labile in the mitochondria, i.e. not incorporated into complex IV, it binds to the copper probe and the orange emission peak is sensitive to copper concentration. Therefore, a higher fluorescence intensity would suggest a decrease in unbound mitochondrial copper (thus a suggested increase in incorporated copper), while a lower fluorescence intensity would suggest the opposite. We first assessed mitochondrial copper in a subset of *LRRK2*-G2019S manifesting, non-manifesting and control fibroblasts. As seen in Figure 7a and 7b, there were no observable or quantifiable differences in mitochondrial copper between the different cell lines. However, this finding does not rule out changes in mitochondrial copper being present in other patient derived lines which were not tested or indeed the probe not being sensitive enough in this cell type.

It must be considered that the mitochondria are not the only compartment where copper is important in the cell. Therefore, cytosolic copper was assessed using a cytosolic copper probe NS2-AI-SiR. Cytosolic copper was assessed in *LRRK2*-G2019S manifesting, non-manifesting and control fibroblasts, and no difference was found (Figure 7c and 7d). The lack of differences in unbound mitochondrial or cytosolic copper in the *LRRK2*-G2019S manifesting fibroblasts compared to control cells could suggest that the SCO2 expression deficit seen in these lines does not affect the transfer of copper to complex IV and that the SCO2 deficit in this cohort could be resulting in other deficiencies. However, further work would need to be undertaken to show no differences in copper across the whole cohort. Previous literature suggests that a loss of SCO2 can cause a reduction in cellular respiration which in turn affects redox homeostasis, leading to an increase in ROS production in HCT116 cells (44). However, we did not see a significant increase in ROS production in the *LRRK2*-G2019S manifesting fibroblast lines compared to control, the cohort which presented the SCO2 deficit, suggesting that this could be a cell type dependent observation.

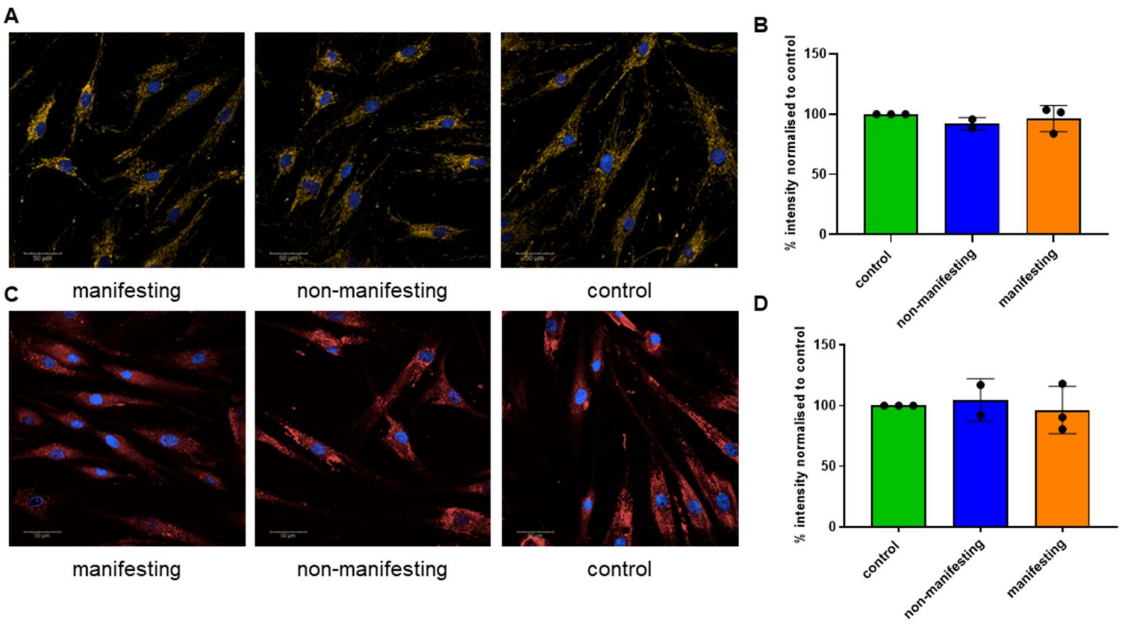


**Figure 7 - Mitochondrial and cytosolic copper in *LRRK2*-G2019S manifesting, non-manifesting and control fibroblasts.** (**a**) Representative images of mitochondrial copper InCCu1 probe in *LRRK2*-G2019S manifesting, non-manifesting and control fibroblasts. (**b**) Percentage of mitochondrial copper probe intensity normalised to control fibroblasts. N=3 *LRRK2*-G2019S manifesting, 2 *LRRK2*-G2019S non-manifesting, 5 control cell lines. Each dot represents the mean of the experimental repeats per line for lines with 3 biological repeats. (**c**) Representative images of cytosolic copper NS2-AI-SiR probe in *LRRK2*-G2019S manifesting, non-manifesting and control fibroblasts. (**d**) Graph represents percentage of cytosolic copper probe intensity normalised to control fibroblasts n=3 *LRRK2*-G2019S manifesting, 2 *LRRK*-G2019S non-manifesting, 4 control cell lines. Each dot represents the mean of the experimental repeats per line for lines with at least 2 biological repeats. On average, 150-300 cells per cell line, per condition for each repeat were analysed. Results represent at least 2 technical repeats. Results expressed as the mean ± SD. Scale bar, 50 µm.

## Discussion

Here, we present data from one of the largest G2019S *LRRK2*-PD manifesting and non-manifesting cohorts of fibroblasts studied thus far. We show a variable mitochondrial phenotype when assessing global mitochondrial measures such as cellular ATP levels and MMP. However, culture in galactose media revealed more pronounced changes in the *LRRK2*-G2019S fibroblasts. The data from this expanded cohort reveals less significant and homogenous reductions in cellular ATP and MMP than have previously been shown. However, this could be due to the shorter growth time in galactose media used in this study (24 hours), as fibroblasts in previous studies revealing significant and robust reductions were cultured for 72 hours (17). It has previously been reported that ATP deficits are revealed at varying degrees over a period of 24 to 72 h in OXPHOS defective optic neuropathy fibroblasts (45). We chose 24-hour galactose exposure in this study to minimise differences in cell growth across such a large cohort of samples. Glucose deprivation has also been reported to moderately increase LRRK2 kinase activity; however, the intracellular depletion of ATP resulted in changes in LRRK2 phosphorylation in primary astrocytes (46), this has not been investigated in fibroblasts to date. G2019S-*LRRK2* phosphorylation in the context of reduced cellular ATP levels in patient-derived cellular models may be interesting to explore to further elucidate the penetrance of the G2019S mutation. The data here, in an expanded cohort measuring MMP, shows no significant group changes with variable MMP between different patient lines. Whilst most studies previously investigating MMP have found deficiencies, this is not the case for all studies, hence some differences may exist between patients with some patients having compensatory mechanisms (47)(15)(17)(36)(48).

Dysfunctional mitochondria have been shown to produce an increased amount of ROS (49) with ROS being suggested as a major mechanism by which LRRK2 elicits cellular changes (50). Here, we observed a small, but non-significant, increase in mitochondrial ROS in some of the *LRRK2*-G2019S manifesting cell lines, while no differences were found between the different subgroups in cytosolic ROS.

There is minimal literature exploring ROS specifically in *LRRK2*-G2019S fibroblasts, with conflicting evidence. Yakhine-Diop et al. 2019 found an increase in ROS production and mitochondrial ROS in *LRRK2* patient fibroblasts, while Papkovskaia et al. 2012 observed that intracellular ROS generation rate was decreased in *LRRK2*-G2019S patient fibroblasts (51)(47). Su and Qi, 2013 found a variable increase in mitochondrial ROS in three LRRK2-G2019S patient fibroblasts compared with one control line (37). The variability in ROS measurements in the literature can also depend on the specific ROS probes used for each measurement.

Interestingly, the trend towards a strong decrease in a complex IV subunits expression in our study has also been published in other studies investigating the *LRRK2*-G2019S mutation. For example, Su and Qi 2013 also used the same OXPHOS antibody and found decreased protein expression in both complex I and complex IV in HeLa cells overexpressing *LRRK2*-G2019S (37). Our study identified a decrease in NDUFB8 expression, a complex I submit in four of the six *LRRK2*-G2019S manifesting cell lines. In future studies it may also be insightful to also look at additional complex I subunits to see whether our result is restricted to NDUFB8 or if it occurs globally across other complex I subunits. To further elucidate OXPHOS activity in relation to *LRRK2*-G2019S penetrance, future studies could investigate oxygen consumption and specific mitochondrial respiration via the Seahorse and Resipher assays to give further insight into the metabolic activity of this cohort of patient-derived fibroblasts.

A particularly interesting finding in our study was the significant decrease in SCO2 expression in *LRRK2*-G2019S PD fibroblasts which did not correlate with a change in unbound mitochondrial or cytosolic copper or ROS in a limited cohort. It is important to note that the copper analysis in this study was only undertaken in a small sample of our *LRRK2*-G2019S cohort. Future studies would benefit from investigating the unbound mitochondrial and cytosolic copper in the full *LRRK2*-G2019S cohort to fully elucidate whether decreases in SCO2 expression are causative of unbound copper in *vitro*. Furthermore, a full validation of the probe's responsiveness to bound and unbound copper changes in primary fibroblasts is needed to robustly interpret the findings.

To our knowledge, SCO2 deficiency has thus far not been reported in PD. However, there are several cases where *SCO2* mutations are pathogenic. Mutations in *SCO2* have been associated with fatal infantile cardioencephalomyopathy, myopia, Leigh syndrome, cerebellar ataxia and progressive peripheral axonal neuropathy, and early-onset axonal Charcot-Marie-Tooth disease (52)(53)(54)(55)(56)(57)). There is evidence to suggest that *SCO2* mutations lead to a decrease in COXII expression, mitochondrial complex IV activity and cellular copper levels (58)(59)(60). Dodani et al. 2011 explored both cellular and mitochondrial copper in SCO2 patient fibroblasts using a targetable fluorescent sensor Mito-CS1 (61). They found that though there was a global decrease in cellular copper, labile mitochondrial $Cu^{+}$ in SCO2 patient fibroblasts was largely unaltered.

Epidemiological studies in PD have shown that long-term metal exposure, including copper, increases the risk of developing PD (62). It has been proposed that copper could increase oxidative stress by converting superoxide anion and hydrogen peroxide into the hydroxyl radical, which is considered the most reactive oxygen species (63). Copper has also been

demonstrated to increase the oxidation process of dopamine and has a role in the promotion of alpha-synuclein aggregation (64)(65). Multiple studies have shown that there is a substantial decrease in copper levels specifically in the substantia nigra of patients with PD (66)(67)(68). Overall, it is clear that a balance of copper is required for normal physiological function, and dysfunction of this balance is associated with PD, and this may be altered in other cell types by reductions in SCO2. HERC2 is a ubiquitin ligase which has been shown to interact both with SCO2 and LRRK2, thus this may provide the mechanistic link as to how *LRRK2* mutations cause a reduction in SCO2 (69)(70).As endogenous expression levels of HERC2 and LRRK2 are relatively low in fibroblasts, future studies could investigate the expression and associated mechanisms of proteins assessed in this study in an alternative in vitro model such as patient-derived induced dopaminergic neurons to fully recapitulate *LRRK2*-G2019S penetrance in a cell type directly implicated in PD with higher endogenous LRRK2 expression (71).

As mentioned previously, there is a benefit in studying an expanded cohort of non-manifesting *LRRK2*-G2019S patients due to the pre-clinical nature of this cohort. The non-manifesting cohort were heterogeneous in both mitochondrial function and morphology. For example, one non-manifesting line showed a particularly severe ATP deficit when exposed to galactose media. The mild changes identified here in mitochondrial morphology could also be due to using live imaging labelling of mitochondria rather than other assessments of mitochondrial morphology not reliant on live imaging fluorescent dyes. In addition, a subset of the non-manifesting lines showed an increase in SCO2 expression and a decrease in DRP1 expression. This may suggest a compensatory effect in some of the non-manifesting cohort. A recent study involving control and *LRRK2*-G2019S iPSC-derived astrocytes also found a decrease in DRP1 protein expression in *LRRK2* mutant astrocytes, which reinforces the decrease in DRP1 expression we see in some non-manifesting lines (72). Biological heterogeneity was also apparent in the manifesting group in terms of cellular ROS and mitochondrial localisation representing the variation within symptomatic *LRRK2*-G2019S PD patients, even with a shared LRRK2 mutation. This highlights the importance of studying expanded cohorts, specifically of patient-derived cells, to fully examine the natural heterogeneity of PD patients.

It is important to acknowledge that the non-manifesting cohort is on average younger than the manifesting *LRRK2*-G2019S cohort in this study. Given that *LRRK2*-G2019S penetrance is age-dependent, it is plausible that our non-manifesting cohort includes pre-symptomatic individuals, which may progress to the manifesting cohort with age. Thus, it is possible that the SCO2 reduction observed here in the manifesting cohort could be attributable to age-related factors rather than actual *LRRK2*-G2109S penetrance. Therefore, it would be interesting in future studies to determine whether age of *LRRK2*-G2019S PD onset is correlated with mitochondrial dysfunction and OXPHOS subunit and assembly factor deficiencies. This study may point towards the need for a precision medicine approach moving forward. While this is one of the largest studies in patient-derived cells reported for *LRRK2*-G2019S mutation carriers, it could be expanded further to include more participant lines from both the manifesting and non-manifesting cohorts, as well as investigation of other cell types. It is important to note the utility of fibroblasts in understanding disease related mechanisms, patient derived fibroblasts retain the epigenetic changes which build up over a person's lifetime. In addition, all proteins are expressed at endogenous levels, therefore fibroblasts have an important place in adding to our understanding of disease mechanisms and patient variability leading to precision medicine approaches for complex diseases.

Limitations

Whilst our study uses one of the largest cohorts of patient derived fibroblast lines from LRRK2-G2019S carriers for many of our assays, there are multiple limitations to our study. We did not undertake all of the experimental investigations in the entire cohort, limiting our investigations of copper for example to a smaller subset of lines. This is a limitation of the study and means that we cannot rule out changes in mitochondrial or cytosolic copper are present as a result of the changes in Sco2 expression. Furthermore, some of the methods utilised in this study would be strengthened by orthogonal assessments, including mitochondrial morphology changes assessed using other methods than live imaging and investigation of submits of each of the respiratory chain complexes.

## Conclusions

Our study shows the possible heterogeneity of cellular phenotype of *LRRK2*-G2019S mutation carriers, which could be important in future clinical trials for both LRRK2 ASOs and kinase inhibitors, in addition to genetic screening of idiopathic patients included in clinical trials.

## Methods

### Patient and control fibroblast lines and culture

8 skin biopsies were taken from LRRK2 manifesting (63.0 ± 9.0 years), 8 LRRK2 non-manifesting (51.0 ± 15.9 years) and 13 controls (60 ± 13.1 years; Table S1) and were cultured until fibroblasts began to grow. These biopsies were set up in Trondheim, Norway, in line with local ethics (Ethical approval no. 4.2008.414). All experimental protocols were approved by Department of Neurology, St Olav's Hospital, Trondheim, Norway ethics committee. All experiments were performed in accordance with relevant guidelines and regulations. Informed consent was obtained from all subjects and/or their legal guardian(s). Two fibroblast lines were also obtained from the Coriell Cell repository (Camden, New Jersey, USA) under MTA. All lines were cultured in Eagle's Minimum Essential Medium (EMEM) (Lonza) supplemented with 10% Foetal Bovine Serum (FBS) (Biosera), 1% Minimum Essential Medium (MEM) vitamins (Lonza), 1% penicillin/streptomycin (Lonza), 1% sodium pyruvate (Sigma), 1% non-essential amino acids (Lonza), and 50 mg/ml uridine (Sigma). Cells were routinely tested for *Mycoplasma* contamination. In selected experiments, media containing galactose instead of glucose was used for 24h prior to the assay. For this Dulbecco's Modified Eagle's Medium (DMEM) without glucose (Gibco) was supplemented with 10% FBS (Biosera), 1% MEM vitamins (Lonza), 1% penicillin/streptomycin (Lonza), 1% sodium pyruvate (Sigma), 1% non-essential amino acids (Lonza), 500 µl uridine (50 mg/ml) (Sigma), and 0.9 mg/ml of galactose (Sigma).

### ATP assay

Cells were plated overnight at a density of 5000 cells per well of a white 96 well plate (Greiner BioOne). After adding galactose media to the allocated wells for 24h, ATP levels were measured using the ATPlite kit (Perkin Elmer) as per the manufacturer's instructions and previously published methods (16). Luminescence was read on the PHERAstar FS or Omega plate reader (BMG Labtech). ATP values were normalised to cell number using Cyquant (ThermoFisher).

### Mitochondrial membrane potential assay

To measure MMP, 2000 cells per well were plated overnight in a black 96 well plate (Perkin Elmer). After adding galactose media to the allocated wells for 24h, some wells from each line were incubated with 10 µM carbonyl cyanide m-chlorophenyl hydrazine (CCCP) (Sigma) for 1h. All cells were then incubated with 80 nM tetramethylrhodamine, methyl ester (TMRM) (ThermoFisher) and 1 µM Hoechst (Sigma) for 1 h in phenol-red free MEM (ThermoFisher). Cells were imaged using the InCell 2000 high content imager microscope (GE Healthcare) at

37°C and 5% $CO_2$. Images were analysed using a custom protocol in InCell Developer Toolbox (24)(25)(25) (GE Healthcare). In this, individual nuclei and mitochondria were segmented. Short mitochondria were defined as having a form factor >0.4 and long mitochondria were defined as having a form factor <0.4. Form factor is calculated using the equation $(pm^2)/(4\pi am)$ where pm is mitochondrial perimeter length and am is the mitochondrial area.

**Copper and reactive oxygen species probes**

To measure copper and cytosolic and mitochondrial reactive oxygen species, 2000 cells per well were plated overnight in a black 96 well plate (Perkin Elmer). After adding galactose media to the allocated wells for 24h, fibroblasts were incubated with either one of: cytosolic ROS probe (NpFR1, 40 μM)(27), two mitochondrial ROS probes (NpFR2 or FRR2, 40 μM)(28)(29) or one copper probe (InCCu1, 200nM)(30) all for 45 minutes. All cells were also incubated with 1μM Hoechst. To measure cytosolic copper, the probe NS2-AI-SiR was used, which was kindly provided by our collaborator Professor Christopher Chang, University of California, Berkeley. For this probe, cells were incubated with 1 μM Hoechst for 45 minutes followed by 1 μM NS2-AI-SiR for 15 minutes. Cells were imaged using an Opera Phenix High Content Screening System (Revvity), 40x water objective, with a minimum of 12 fields of view per well and at least two technical replicates of each line/condition. FRR2 and InCCu1 were imaged at 561 nm excitation, 570-630 nm emission, NpFr1 and NpFR2 were imaged at 488 nm excitation, 500-550 nm emission, and NS2-AI-SiR was imaged at 640 nm excitation, 650-7600 nm emission.

**Western blotting and antibodies**

Protein quantification of cell lysates was performed using a Bradford assay including BSA (Sigma) standards to produce a standard curve (31). Protein samples of 10 μg protein were run on a 12% resolving gel and stacking gel. Samples were transferred to a Polyvinylidene fluoride (PVDF) membrane (Merck) (32). Membranes were probed with primary antibodies and subsequently with secondary antibodies diluted in TBST (Table S2). Membranes were imaged using G-box (SynGene) and Genetools software (SynGene) was used for densitometry analysis of captured images. Each antibody was normalised to beta-actin as a loading control, before being normalised to untreated control samples. Each membrane contained at least one control fibroblast line for normalisation.

**Immunofluorescent staining**

Cells were fixed using 4% paraformaldehyde (Merck) diluted in PBS and stored at 4°C in PBS with 0.4% sodium azide. Cells were permeabilised using 0.1% Triton (Sigma) in PBS with Tween 20 (Sigma) 1:1000 (PBST) and then washed in PBST. Cells were then incubated with blocking solution for 1 h, composed of 5% horse serum in PBST (Agilent) before incubation with primary antibody in blocking solution overnight at 4°C (Table S3). Cells were then washed in PBST, before incubating in secondary antibodies diluted in PBST for 1 h at room temperature (Table S3). Cells were washed in PBST, incubated with Hoechst (1 μM) for 2 minutes, washed in PBST, before adding PBS. Cells were imaged using the Opera Phenix High Content Imaging System as described above.

**Image analysis**

Images captured on the Opera Phenix were analysed using Harmony software (Perkin Elmer). Maximal projection images were used for analysis. For all imaging analyses, on average, 150-300 cells per cell line, per condition for each repeat were analysed. Bespoke protocols for segmentation of nuclei, mitochondria, cytosolic and mitochondrial ROS, and image regions inclusive of cell cytoplasm were established. Mitochondrial ROS measurements normalised to total mitochondrial number assessed via quantification of

TOM20 spots in each individual line. For DRP1 assays, we could not directly analyse colocalization of DRP1 and TOM20 using Harmony analysis software, therefore, to assess DRP1 localisation, the number of DRP1 spots that overlapped with TOM20 spots were analysed. Image segmentation and analysis of mitochondrial morphology parameters was normalised to image region using Harmony software, like methods previously published (24)(25)(26).

**Statistical analysis**

GraphPad Prism was used for statistical analysis. $p<0.05$ was deemed significant. For the comparison of two groups either an unpaired t-test with Welch's correction or a Mann-Whitney U test was used. For comparison across multiple groups either a one-way ANOVA with Dunnett's multiple comparisons or a Kruskal Wallis with Dunn post-hoc test was used. Individual p values, n numbers and statistical tests for each figure panel are stated in corresponding figure legends. Specific fibroblast lines used for each assay are detailed in Table S4.

**Declarations**

**Ethics**

All experiments were performed in accordance with relevant guidelines and regulations. Informed consent was obtained from all subjects and/or their legal guardian(s).

**Data Availability**

All data is presented within the manuscript.

**Competing Interests**

**Funding**

**Author Contributions**

**RW**: Validation, Formal Analysis, Investigation, Data Curation, Writing – Original Draft, Writing – Review & Editing, Visualisation
**ES**: Formal Analysis, Writing – Original Draft, Writing – Review & Editing, Visualisation
**HC**: Investigation
**OC**: Investigation
**AK**: Resources, Methodology
**EJN**: Resources, Conceptualisation, Writing – Review & Editing, Funding Acquisition
**JA**: Resources, Methodology
**OB**: Resources, Conceptualisation, Supervision, Funding Acquisition
**HM**: Resources, Methodology, Data Curation, Conceptualisation, Writing – Review & Editing, Supervision, Project Administration, Funding Acquisition

**Acknowledgements**

We are very grateful to all research participants for their help with this study. RW/HM were supported by a Rosetrees Trust grant A1222. RW was supported by a University of Sheffield PhD Scholarship. HM was supported by a Parkinson's UK Senior Research Fellowship F-1301. OC was supported by a Biochemical Society Summer Vacation Studentship. EN was supported by Australian Research Council (DE120102687, DP150100649). JA was supported by the Norwegian Parkinson Foundation. This study/research is funded by the National Institute for Health and Care Research (NIHR) Sheffield Biomedical Research Centre (NIHR203321*). The views expressed are those of the author(s) and not necessarily those of the NIHR or the Department of Health and Social Care.

**References**

1.

Parkinson J. An Essay on the Shaking Palsy. The Journal of Neuropsychiatry and Clinical Neurosciences. 1817 May;14(2):223–36.

2.

Dorsey ER, Elbaz A, Nichols E, Abd-Allah F, Abdelalim A, Adsuar JC, et al. Global, regional, and national burden of Parkinson's disease, 1990–2016: a systematic analysis for the Global Burden of Disease Study 2016. The Lancet Neurology. 2018 Nov;17(11):939–53.

3.

Dijkstra AA, Voorn P, Berendse HW, Groenewegen HJ, Rozemuller AJM, van de Berg WDJ. Stage-dependent nigral neuronal loss in incidental Lewy body and Parkinson's disease. Movement Disorders. 2014 Jul 3;29(10):1244–51.

4.

Ascherio A, Schwarzschild MA. The epidemiology of Parkinson's disease: risk factors and prevention. Lancet Neurol. 2016;15(12):1257–72.

5.

Bruggemann N, Klein C. Parkin Type of Early-Onset Parkinson Disease. In: Adam MP, Bick S, Mirzaa GM, Pagon RA, Wallace SE, Amemiya A, editors. GeneReviews((R)). Seattle (WA)1993.

6.

Rui Q, Ni H, Li D, Gao R, Chen G. The Role of LRRK2 in Neurodegeneration of Parkinson Disease. Curr Neuropharmacol. 2018;16(9):1348–57.

7.

Drolet RE, Sanders JM, Kern JT. Leucine-Rich Repeat Kinase 2 (LRRK2) Cellular Biology: A Review of Recent Advances in Identifying Physiological Substrates and Cellular Functions. Journal of Neurogenetics. 2011 Nov 11;25(4):140–51.

8.

Saunders-Pullman R, Raymond D, Wise A. LRRK2 Parkinson Disease [Internet]. PubMed. Seattle (WA): University of Washington, Seattle; 1993. Available from: https://www.ncbi.nlm.nih.gov/books/NBK1208/

9.

Kalia LV, Lang AE, Hazrati LN, Fujioka S, Wszolek ZK, Dickson DW, et al. Clinical correlations with Lewy body pathology in LRRK2-related Parkinson disease. JAMA Neurol. 2015;72(1):100–5.

10.

West AB, Moore DJ, Biskup S, Bugayenko A, Smith WW, Ross CA, et al. Parkinson's disease-associated mutations in leucine-rich repeat kinase 2 augment kinase activity. Proc Natl Acad Sci U S A. 2005;102(46):16842–7.

11.

Healy DG, Falchi M, O'Sullivan SS, Bonifati V, Durr A, Bressman S, et al. Phenotype, genotype, and worldwide genetic penetrance of LRRK2-associated Parkinson's disease: a case-control study. The Lancet Neurology. 2008 Jul;7(7):583–90.
12.
Latourelle JC, Sun M, Lew MF, Suchowersky O, Klein C, Golbe LI, et al. The Gly2019Ser mutation in LRRK2is not fully penetrant in familial Parkinson's disease: the GenePD study. BMC Medicine. 2008 Nov 5;6(1).
13.
Biskup S, Moore DJ, Celsi F, Higashi S, West AB, Andrabi SA, et al. Localization of LRRK2 to membranous and vesicular structures in mammalian brain. Annals of Neurology. 2006 Nov;60(5):557–69.
14.
Wallings R, Manzoni C, Bandopadhyay R. Cellular processes associated with LRRK2 function and dysfunction. FEBS Journal. 2015 May 9;282(15):2806–26.
15.
Grünewald A, Arns B, Meier B, Brockmann K, Tadic V, Klein C. Does Uncoupling Protein 2 Expression Qualify as Marker of Disease Status in LRRK2-Associated Parkinson's Disease? Antioxidants & Redox Signaling. 2014 May;20(13):1955–60.
16.
Mortiboys H, Johansen KK, Aasly JO, Bandmann O. Mitochondrial impairment in patients with Parkinson disease with the G2019S mutation in LRRK2. Neurology. 2010 Nov 29;75(22):2017–20.
17.
Mortiboys H, Furmston R, Bronstad G, Aasly J, Elliott C, Bandmann O. UDCA exerts beneficial effect on mitochondrial dysfunction inLRRK2G2019Scarriers and in vivo. Neurology. 2015 Aug 7;85(10):846–52.
18.
Ramonet D, Daher JPL, Lin BM, Stafa K, Kim J, Banerjee R, et al. Dopaminergic Neuronal Loss, Reduced Neurite Complexity and Autophagic Abnormalities in Transgenic Mice Expressing G2019S Mutant LRRK2. PLoS ONE. 2011 Apr 6;6(4):e18568.
19.
Yue M, Hinkle KM, Davies P, Trushina E, Fiesel FC, Christenson TA, et al. Progressive dopaminergic alterations and mitochondrial abnormalities in LRRK2 G2019S knock-in mice. Neurobiol Dis. 2015;78:172–95.
20.

Ho DH, Je AR, Lee H, Son I, Kweon HS, Kim HG, et al. LRRK2 Kinase Activity Induces Mitochondrial Fission in Microglia via Drp1 and Modulates Neuroinflammation. Exp Neurobiol. 2018;27(3):171–80.
21
Zhao HT, John N, Delic V, Ikeda-Lee K, Kim A, Weihofen A, et al. LRRK2 Antisense Oligonucleotides Ameliorate alpha-Synuclein Inclusion Formation in a Parkinson's Disease Mouse Model. Mol Ther Nucleic Acids. 2017;8:508–19.
22.
Wallings RL, Mark JR, Staley HA, Gillett DA, Neighbarger N, Kordasiewicz H, et al. ASO-mediated knockdown or kinase inhibition of G2019S-Lrrk2 modulates lysosomal tubule-associated antigen presentation in macrophages. Mol Ther Nucleic Acids. 2023;34:102064.
23.
Pena N, Richbourg T, Gonzalez-Hunt CP, Qi R, Wren P, Barlow C, et al. G2019S selective LRRK2 kinase inhibitor abrogates mitochondrial DNA damage. NPJ Parkinsons Dis. 2024;10(1):49.
24.
Diot A, Hinks-Roberts A, Lodge T, Liao C, Dombi E, Morten K, et al. A novel quantitative assay of mitophagy: Combining high content fluorescence microscopy and mitochondrial DNA load to quantify mitophagy and identify novel pharmacological tools against pathogenic heteroplasmic mtDNA. Pharmacological Research. 2015 Oct;100:24–35.
25.
Carling PJ, Mortiboys H, Green C, Simeon Mihaylov, Sandor C, Aurelie Schwartzentruber, et al. Deep phenotyping of peripheral tissue facilitates mechanistic disease stratification in sporadic Parkinson’s disease. Progress in Neurobiology. 2020 Apr 1;187:101772–2.
26.
Payne T, Burgess T, Bradley S, Roscoe S, Sassani M, Dunning MJ, et al. Multimodal assessment of mitochondrial function in Parkinson's disease. Brain. 2024;147(1):267–80.
27.
Yeow J, Kaur A, Anscomb MD, New EJ. A novel flavin derivative reveals the impact of glucose on oxidative stress in adipocytes. Chem Commun (Camb). 2014;50(60):8181–4.
28.
Kaur A, Kurt, Cashman TF, Fraser ST, New EJ. Mitochondrially targeted redox probe reveals the variations in oxidative capacity of the haematopoietic cells. Organic & Biomolecular Chemistry. 2015 Jan 1;13(24):6686–9.
29.

Kaur A, Karolina Jankowska, Pilgrim C, Fraser ST, New EJ. Studies of Hematopoietic Cell Differentiation with a Ratiometric and Reversible Sensor of Mitochondrial Reactive Oxygen Species. Antioxidants and Redox Signaling. 2016 May 1;24(13):667–79.
30.
Shen C, Kolanowski JL, Tran CMN ., Kaur A, Akerfeldt MC, Rahme MS, et al. A ratiometric fluorescent sensor for the mitochondrial copper pool. Metallomics. 2016;8(9):915–9.
31.
Bradford MM. A rapid and sensitive method for the quantitation of microgram quantities of protein utilizing the principle of protein-dye binding. Anal Biochem. 1976;72:248–54.
32.
Mozdzanowski J, Hembach P, Speicher DW. High yield electroblotting onto polyvinylidene difluoride membranes from polyacrylamide gels. Electrophoresis. 1992;13(1):59–64.
33.
Götz Hofhaus, Johns DR, Orest Hurko, Attardi G, Chomyn A. Respiration and Growth Defects in Transmitochondrial Cell Lines Carrying the 11778 Mutation Associated with Leber's Hereditary Optic Neuropathy. Journal of Biological Chemistry. 1996 May 31;271(22):13155–61.
34.
Heo HY, Park JM, Kim CH, Han BS, Kim KS, Seol W. LRRK2 enhances oxidative stress-induced neurotoxicity via its kinase activity. Exp Cell Res. 2010;316(4):649–56.
35.
Wang X, Yan MH, Fujioka H, Liu J, Wilson-Delfosse A, Chen SG, et al. LRRK2 regulates mitochondrial dynamics and function through direct interaction with DLP1. Human Molecular Genetics. 2012 Jan 6;21(9):1931–44.
36.
Walter J, Bolognin S, Antony PMA, Nickels SL, Poovathingal SK, Salamanca L, et al. Neural Stem Cells of Parkinson's Disease Patients Exhibit Aberrant Mitochondrial Morphology and Functionality. Stem Cell Reports. 2019 May;12(5):878–89.
37.
Su YC, Qi X. Inhibition of excessive mitochondrial fission reduced aberrant autophagy and neuronal damage caused by LRRK2 G2019S mutation. Human Molecular Genetics. 2013 Jun 27;22(22):4545–61.
38.
Perez Carrion M, Pischedda F, Biosa A, Russo I, Straniero L, Civiero L, et al. The LRRK2 Variant E193K Prevents Mitochondrial Fission Upon MPP+ Treatment by Altering LRRK2 Binding to DRP1. Frontiers in Molecular Neuroscience. 2018 Feb 28;11(64).
39.

Anand R, Wai T, Baker MJ, Kladt N, Schauss AC, Rugarli E, et al. The i-AAA protease YME1L and OMA1 cleave OPA1 to balance mitochondrial fusion and fission. J Cell Biol. 2014;204(6):919–29.

40.

Wang R, Mishra P, Garbis SD, Moradian A, Sweredoski MJ, Chan DC. Identification of new OPA1 cleavage site reveals that short isoforms regulate mitochondrial fusion. Molecular Biology of the Cell. 2021 Jan 15;32(2):157–68.

41.

Michalska BM, Kwapiszewska K, Szczepanowska J, Kalwarczyk T, Patalas-Krawczyk P, Szczepański K, et al. Insight into the fission mechanism by quantitative characterization of Drp1 protein distribution in the living cell. Scientific Reports. 2018 May 25;8(1).

42.

Leary SC, Sasarman F, Nishimura T, Shoubridge EA. Human SCO2 is required for the synthesis of CO II and as a thiol-disulphide oxidoreductase for SCO1. Human Molecular Genetics. 2009 Mar 31;18(12):2230–40.

43.

Álvarez C, Marín-Buera L, M. Carmen Gil-Borlado, Rivera H, Blázquez A, Seneca S, et al. Cellular pathophysiological consequences of BCS1L mutations in mitochondrial complex III enzyme deficiency. Human Mutation. 2010 Aug 1;31(8):930–41.

44.

Sung HJ, Ma W, Wang PY, Hynes J, O'Riordan TC, Combs CA, et al. Mitochondrial respiration protects against oxygen-associated DNA damage. Nat Commun. 2010;1:5.

45.

Pasqualotto BA, Tegeman C, Frame AK, McPhedrain R, Halangoda K, Sheldon CA, et al. Galactose-replacement unmasks the biochemical consequences of the G11778A mitochondrial DNA mutation of LHON in patient-derived fibroblasts. Exp Cell Res. 2024;439(1):114075.

46.

Kentros M, Follett J, Subrahmanian N, Chairmandurai A, Melachroinou K, Re DB, et al. Regulation of LRRK2 activity by metabolic stress and heavy metal exposure. Brain Res. 2025;1863:149785.

47.

Papkovskaia TD, Chau KY, Inesta-Vaquera F, Papkovsky DB, Healy DG, Nishio K, et al. G2019S leucine-rich repeat kinase 2 causes uncoupling protein-mediated mitochondrial depolarization. Hum Mol Genet. 2012;21(19):4201–13.

48.

Ludtmann MHR, Kostic M, Horne A, Gandhi S, Sekler I, Abramov AY. LRRK2 deficiency induced mitochondrial Ca2+ efflux inhibition can be rescued by Na+/Ca2+/Li+ exchanger upregulation. Cell Death & Disease. 2019 Mar 19;10(4).
49.
Park JS, Davis RL, Sue CM. Mitochondrial Dysfunction in Parkinson's Disease: New Mechanistic Insights and Therapeutic Perspectives. Current Neurology and Neuroscience Reports. 2018 Apr 3;18(5).
50.
Keeney MT, Rocha EM, Hoffman EK, Farmer K, Maio RD, Weir J, et al. LRRK2 regulates production of reactive oxygen species in cell and animal models of Parkinson's disease. Science Translational Medicine. 2024 Oct 2;16(767).
51.
Sokhna M. S. Yakhine-Diop, Mireia Niso-Santano, Rodríguez-Arribas M, Rubén Gómez-Sánchez, Martínez-Chacón G, Elisabet Uribe-Carretero, et al. Impaired Mitophagy and Protein Acetylation Levels in Fibroblasts from Parkinson's Disease Patients. Molecular neurobiology. 2018 Jul 21;56(4):2466–81.
52.
Papadopoulou LC, Sue CM, Davidson MM, Tanji K, Nishino I, Sadlock JE, et al. Fatal infantile cardioencephalomyopathy with COX deficiency and mutations in SCO2, a COX assembly gene. Nature Genetics. 1999 Nov;23(3):333–7.
53.
Jaksch M, Ogilive I, Yao J, Kortenhaus G, Bresser H-G, Gerbitz K-D, et al. Mutations in SCO2 are associated with a distinct form of hypertrophic cardiomyopathy and cytochrome c oxidase deficiency. Human Molecular Genetics. 2000 Mar 22;9(5):795–801.
54.
Tran-Viet KN, Powell C, Barathi Veluchamy A, Klemm T, Maurer-Stroh S, Limviphuvadh V, et al. Mutations in SCO2 Are Associated with Autosomal-Dominant High-Grade Myopia. The American Journal of Human Genetics. 2013 May;92(5):820–6.
55.
Ruhoy IS, Saneto RP. The genetics of Leigh syndrome and its implications for clinical practice and risk management. Appl Clin Genet. 2014;7:221–34.
56.
Rebelo AP, Saade D, Pereira CV, Farooq A, Huff TC, Abreu L, et al. SCO2 mutations cause early-onset axonal Charcot-Marie-Tooth disease associated with cellular copper deficiency. Brain. 2018 Jan 16;141(3):662–72.
57.

Barcia G, Zahra Assouline, Pennisi A, Gitiaux C, Schiff M, Boddaert N, et al. Cytochrome c oxidase deficiency caused by biallelic SCO2 mutations in two sibs with cerebellar ataxia and progressive peripheral axonal neuropathy. Molecular Genetics and Metabolism Reports. 2019 Nov 6;21:100528–8.

58.

Jaksch M, Paret C, Stucka R, Horn N, Muller-Hocker J, Horvath R, et al. Cytochrome c oxidase deficiency due to mutations in SCO2, encoding a mitochondrial copper-binding protein, is rescued by copper in human myoblasts. Human Molecular Genetics. 2001 Dec 1;10(26):3025–35.

59.

Leary SC, Cobine PA, Kaufman BA, Guercin GH, Mattman A, Palaty J, et al. The Human Cytochrome c Oxidase Assembly Factors SCO1 and SCO2 Have Regulatory Roles in the Maintenance of Cellular Copper Homeostasis. Cell Metabolism. 2007 Jan;5(1):9–20.

60.

Yang HG, Brosel S, Acín-Pérez R, Vesna Slavkovich, Nishino I, Khan RS, et al. Analysis of mouse models of cytochrome c oxidase deficiency owing to mutations in Sco2. Human Molecular Genetics. 2009 Oct 16;19(1):170–80.

61.

Dodani SC, Leary SC, Cobine PA, Winge DR, Chang CJ. A Targetable Fluorescent Sensor Reveals That Copper-DeficientSCO1andSCO2Patient Cells Prioritize Mitochondrial Copper Homeostasis. Journal of the American Chemical Society. 2011 Jun 8;133(22):8606–16.

62.

Montgomery EB. Heavy metals and the etiology of Parkinson's disease and other movement disorders. Toxicology. 1995 Mar;97(1-3):3–9.

63.

Bisaglia M, Bubacco L. Copper Ions and Parkinson's Disease: Why Is Homeostasis So Relevant? Biomolecules. 2020 Jan 29;10(2):195.

64.

Wang X, Moualla D, Wright JA, Brown DR. Copper binding regulates intracellular alpha-synuclein localisation, aggregation and toxicity. Journal of Neurochemistry. 2010 May;113(3):704–14.

65.

Pham AN, Waite TD. Cu(II)-catalyzed oxidation of dopamine in aqueous solutions: Mechanism and kinetics. Journal of Inorganic Biochemistry. 2014 Aug;137:74–84.

66.

Dexter DT, Wells FR, Lee AJ, Agid F, Agid Y, Jenner P, et al. Increased Nigral Iron Content and Alterations in Other Metal Ions Occurring in Brain in Parkinson's Disease. Journal of Neurochemistry. 1989 Jun;52(6):1830–6.
67.
Riederer P, Sofic E, Rausch WD, Schmidt B, Reynolds GP, Jellinger K, et al. Transition Metals, Ferritin, Glutathione, and Ascorbic Acid in Parkinsonian Brains. Journal of Neurochemistry. 1989 Feb;52(2):515–20.
68.
Genoud S, Roberts BR, Gunn AP, Halliday GM, Lewis SJG, Ball HJ, et al. Subcellular compartmentalisation of copper, iron, manganese, and zinc in the Parkinson's disease brain. Metallomics. 2017;9(10):1447–55.
69.
Locatelli M, Farina C. Role of copper in central nervous system physiology and pathology. Neural Regen Res. 2025;20(4):1058–68.
70.
Gale J, Aizenman E. The physiological and pathophysiological roles of copper in the nervous system. European journal of neuroscience/EJN European journal of neuroscience. 2024 May 15;60(1):3505–43.
71.
Russo I, Kaganovich A, Ding J, Landeck N, Adamantios Mamais, Varanita T, et al. Transcriptome analysis of LRRK2 knock-out microglia cells reveals alterations of inflammatory- and oxidative stress-related pathways upon treatment with α-synuclein fibrils. Neurobiology of Disease. 2019 May 15;129:67–78.
72.
Ding M, Wang F, Jiang LL, Ma C, Qi YW, Liu JY, et al. LRRK2 G2019S mutation contributes to mitochondrial transfer dysfunction in a Drp1-STX17-dependent manner. Transl Neurodegener. 2025;14(1):64.